IOP Publishing Superconductor Science and Technology
Supercond. Sci. Technol. 33 (2020) 024005 (12pp) https://doi.org/10.1088/1361-6668/ab6244

Short-circuit fault current-limiting characteristics of a resistive-type superconducting fault current limiter in DC grids

Bin Xiang, Lei Gao, Zhiyuan Liu, Yingsan Geng and Jianhua Wang

State Key Laboratory of Electrical Insulation and Power Equipment, Department of Electrical Engineering, Xi'an Jiaotong University, Xi'an, People's Republic of China

E-mail: xiangbin0319@163.com

Received 10 October 2019, revised 2 December 2019
Accepted for publication 16 December 2019
Published 8 January 2020

Abstract

Resistive-type superconducting fault current limiters (R-SFCLs) can limit short-circuit fault current and help DC circuit breakers (DCCBs) to isolate short-circuit faults in medium voltage and high voltage DC (HVDC) systems. SFCLs are always used with circuit breakers to break short-circuit current in power systems. The interruption characteristics of the DCCBs influence the current-limiting characteristics of the SFCLs. However, there has been a lack of investigation into the current-limiting and interruption characteristics when R-SFCLs are combined with mechanical-type DCCBs (M-DCCBs) based on the self-excited oscillation interruption principle in medium voltage and HVDC systems. The objective of this paper is to obtain the short-circuit fault current-limiting characteristics of a designed R-SFCL combined with an M-DCCB in DC grids. This paper describes the design of a 10 kV DC R-SFCL which was tested in combination with an M-DCCB in a DC circuit in order to obtain the quenched resistance and the required current interruption characteristics. Besides, a modular multilevel converter-based multi-terminal direct current (MMC-MTDC) grid was used to investigate the current-limiting and interrupting characteristics of the R-SFCL and the M-DCCB in a realistic HVDC grid. The experimental results show that in the 10 kV DC circuit the R-SFCL combined with the M-DCCB limited a 10 kA DC to the peak value of 1416 A and then interrupted this limited current successfully. And unlike other methods of DC interruption, this did not create overvoltage after interruption. The highest voltage on the R-SFCL is the system voltage during interruption. This means that the R-SFCL can effectively delay the voltage drop in MMC-MTDC grids, and provide enough time for the M-DCCB to interrupt the limited current. Thus, a combination of R-SFCLs and M-DCCBs might be an effective and reliable method to interrupt short-circuit fault currents in medium voltage and HVDC grids.

Keywords: DC circuit breakers, fault current-limiting, HVDC systems, quenched resistance, resistive-type superconducting fault current limiter

(Some figures may appear in colour only in the online journal)

Nomenclature

R-SFCL	Resistive-type superconducting fault current limiter
DCCB	DC circuit breakers
HVDC	High voltage DC
M-DCCB	Mechanical-type DCCBs

MMC	Modular multilevel converter
MTDC	Multi-terminal direct current
VSC	Voltage-source converter
I-SFCL	Inductive-type superconducting fault current limiter
FRT	Fault ride-through
YBCO	$YBa_2Cu_3O_{7-\delta}$
MOA	Metal-oxide arrester
I_m	Limited current
I_{lc}	Current transports in the commutation branch
I_{MOA}	Current transports in MOA
U_{SFCL}	Voltage of the R-SFCL
U_{DCCB}	Voltage of the DCCB
U_{total}	Voltage of the R-SFCL and the DCCB together
I_f	Fault current transports through the R-SFCL

1. Introduction

With the rapid development of DC transmission and distribution systems, the fault currents show a trend of continuous growth. For example, short-circuit fault currents in multi-terminal voltage-source converter (VSC) high voltage DC (HVDC) transmission systems can increase to dozens of kiloamperes within several milliseconds [1]. An extremely high rate of rise and amplitude of the DC short-circuit currents are very hard to break by DC circuit breakers (DCCBs). A superconducting fault current limiter (SFCL) can limit fault currents effectively and delay the voltage decline of converters to provide sufficient time for the DCCBs to interrupt the fault current in DC systems. Chen *et al* introduced inductive-type and resistive-type SFCLs (R-SFCLs) to mitigate the short-circuit current and improve the VSC-HVDC system's transient performance [2, 3]. The simulation results showed that by comparing the specific performance indexes including the current-limiting ratio and restraining capability to voltage/power fluctuations, the R-SFCLs is more preferable than the inductive-type SFCL (I-SFCL) [2, 3]. Lee *et al* studied fault interruption and system recovery characteristics considering three types of fault limiting devices such as an R-SFCL, a saturated iron core SFCL, and a hybrid-type SFCL in combination with DCCBs by simulations [4]. The simulation results showed that, among the three fault limiting devices, the hybrid-type SFCL in combination with a DCCB, delivers the most desirable performance in terms of interruption time, recovery time, energy dissipation, and voltage transients [4]. Liang *et al* proposed a DC hybrid-type SFCL with a two-stage current-limiting capability [5, 6]. In the early stage of a short-circuit fault, the initial transient impulse current is limited by inductance and resistance. In the later stage of a short-circuit fault, a sustained and steady current-limiting resistance is provided by the DC SFCL [5, 6].

R-SFCLs have the ability to limit the rise rate and the amplitude of the short-circuit fault currents to a low level, so that it can relax the interruption requirements for DCCBs [2, 7–9]. Chen *et al* designed an R-SFCL to protect a DC microgrid with wind, photovoltaic, and energy storage [10]. In this case, from the fault analysis, the DC fault current's peak value is suppressed quickly and effectively, and a current-limiting ratio of 63.3% is obtained. The bus voltage is compensated to 62.7% of the nominal level, and the renewable power sources can meet the fault ride-through (FRT) requirements [10]. Xiao *et al* investigated an R-SFCL with a current-limiting resistor of 10 Ω and a response time of 0.1 ms at the negative line of the ±160 kV Qinghui line in China, which can effectively reduce the rapid requirements of cut-off time for DCCBs and improve the converter FRT capability of VSC-HVDC [11]. Saldana *et al* analyzed the impact of R-SFCLs on multi-terminal DC systems and new energy transmission systems. The results showed that R-SFCLs can limit the fault current, protect the converters, and improve the FRT capability [12]. Xiang *et al* investigated the impact of DC current and thermal disturbance on the quench and recovery process of R-SFCLs [13]. Xia *et al* analyzed the magnetic field distribution and electromagnetic force of R-SFCLs with different structures [14]. Zha *et al* investigated recovery time of a solenoid SFCL and a pancake SFCL under different placement modes, and found that the heat dissipation space and the accumulation of bubbles influenced recovery time [15]. Influences of different DC prospective fault currents on quenched resistance, electrical field, and temperature of the R-SFCLs when the R-SFCLs quench and recover have also been studied [16].

The combination of an R-SFCL and a mechanical DCCB (M-DCCB) is an effective method to break DC fault current due to its low power loss, low recovery voltage, high interrupting ability, and high reliability. Yang *et al* proposed a DC current interruption technology for railway DC traction systems, consisting of a DC vacuum circuit breaker with an SFCL [17]. The experimental results showed that the proposed 1.5 kV circuit breaker successfully clears short-circuit faults up to 47 kA by first limiting the prospective current and then interrupting it [17]. A self-charging artificial current zero DCCB is proposed using the voltage of the SFCL to charge the commutation capacitor [18]. The DCCB can interrupt 800 A in a 500 V DC test circuit using LN_2 as the arc-quenching medium [18]. Our group also investigates the current-limiting and interruption characteristics of an SFCL connected to an LN_2 switchgear which can limit the prospective current of 15.7 kA to 800 A and then interrupts the limited current in 2.1 ms [19].

A DCCB including a superconducting current-limiting module and a DC interruption module using the self-excited oscillation interruption principle whas been proposed. The fault current-limiting of the superconducting current-limiting module and the interrupting characteristics of the DC interruption module have been investigated separately by experiments [20, 21].

Until now, there has been a lack of experimental investigation into the current-limiting and interruption characteristics of R-SFCLs combined with M-DCCBs based on

the self-excited oscillation interruption principle in medium voltage and HVDC systems and the effect of interruption on current-limiting is unclear. The objective of this paper is to obtain the short-circuit fault current-limiting characteristics of a designed R-SFCL combined with an M-DCCB in DC grids. This paper describes work to design a 10 kV DC R-SFCL and an M-DCCB which was then combined to obtain the necessary quenched resistance, the current-limiting, and the interruption characteristics. The test DC voltages were 1.3, 3, and 10 kV. The test DC current was from 1–10 kA. The R-SFCL combined with the M-DCCB successfully interrupted 10 kA in the 10 kV DC circuit. Models of the quenched resistances and gas arc were built to investigate temperature, recovery time, and the interrupting characteristics. In addition, modular multilevel converter-based multi-terminal direct current (MMC-MTDC) grids was also applied to investigate the current-limiting and interrupting characteristics of the R-SFCL combined with an M-DCCB in HVDC grids.

2. Experimental setup

2.1. Design of the R-SFCL

The superconducting coils of the R-SFCL are made of $YBa_2Cu_3O_{7-\delta}$ (YBCO) coated conductor tape from American Superconductor Inc. type 8602. The YBCO tape was coated with stainless steel reinforcements and has high resistivity. The YBCO tape has two stainless steel stabilizer layers at the outermost layer of the tape to strengthen the mechanical properties of the tape. The critical current of the tape was 225 A at a self-field of 77 K. The width of the tape was around 12 mm. The resistance per meter of the tape at 293 K was approximately 0.11 $\Omega\,m^{-1}$. When a short-circuit fault occurs, the YBCO tapes need to withstand high fault current. Previous research studies have tested an 8.9 meter-long YBCO tape when the applied DC voltages were 250 and 500 V [22]. The experimental results showed that the 8.9 meter-long YBCO tape could withstand the prospective current from 50–10 kA for 60 ms [22]. After the experiments, the tape was in good condition when the voltage applied on the tape was from 28–56 V m^{-1}. Thus, the voltage applied on the superconducting coils is designed as up to 50 V m^{-1}. The withstand voltage and the quenched resistance are in proportion to the length of the tapes. For the tests of a DC voltage of 10 kV, the length of the tapes should be at least 200 m. The winding methods of the superconducting tapes can be in inductive winding such as solenoid winding or winding in the same direction and non-inductive winding. The non-inductive winding method of the superconducting coils can not only reduce the withstanding force during short-circuit faults, but can also reduce the influence on the current ripple during normal current flow. Thus, the non-inductive winding method is chosen to wind the tapes. The YBCO tapes are winded in an 'S' shape to obtain non-inductance. Figure 1 shows the structure of the pancake plate which is made of nylon as the insulation support for the superconducting coils. The superconducting tapes are installed in slots of the plates. Spacers in the plates are used to separate the superconducting coils for insulation. There are open windows on half of the plates to strengthen the liquid nitrogen (LN_2) flow. After applying the windows, the contact area of the superconducting tapes with LN_2 increases, and LN_2 can flow in the windows to accelerate the heat conduction from the superconducting tapes to the LN_2. The inductance of each plate is measured as approximately 1.9 μH. In all 24 pancake plates are series connected to wind the superconducting coils. Vertical placement can be fixed more conveniently than horizontal placement. And the recovery time is shorter in a vertical placement than it in a horizontal placement [15]. Thus, the superconducting coils are placed vertically to reduce recovery time. Each pancake plate can wind a 9 m long YBCO tape. Thus, the total length of the superconducting coils is 216 m. The highest applied voltage on the tapes is 46.3 V m^{-1}. Table 1 shows the structural parameters of the pancake plates. The pancake plates and the superconducting coils are put in the insulation cylinders

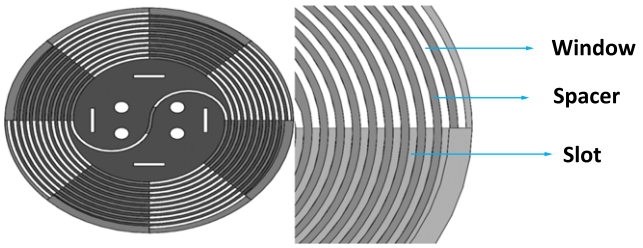

Figure 1. Structure of the pancake plate.

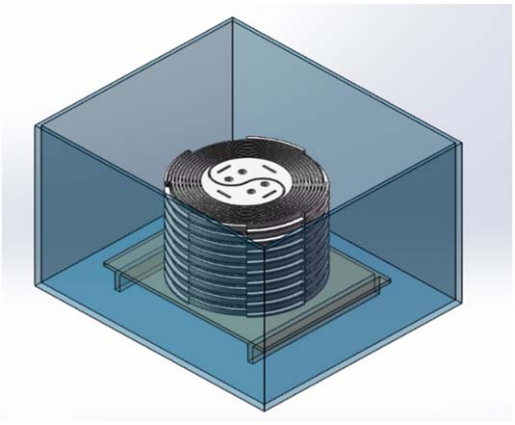

Figure 2. Structure of the insulation cylinder.

Table 1. Structural parameters of the pancake plate.

Specifications	Value
Outside diameter	366 mm
Thickness	20 mm
Slot width	4 mm
Slot depth	12 mm
Minimum bending diameter	100 mm
Spacer width	4 mm
Inductance value	1.9 μH
Resistance value (293 K)	1 Ω

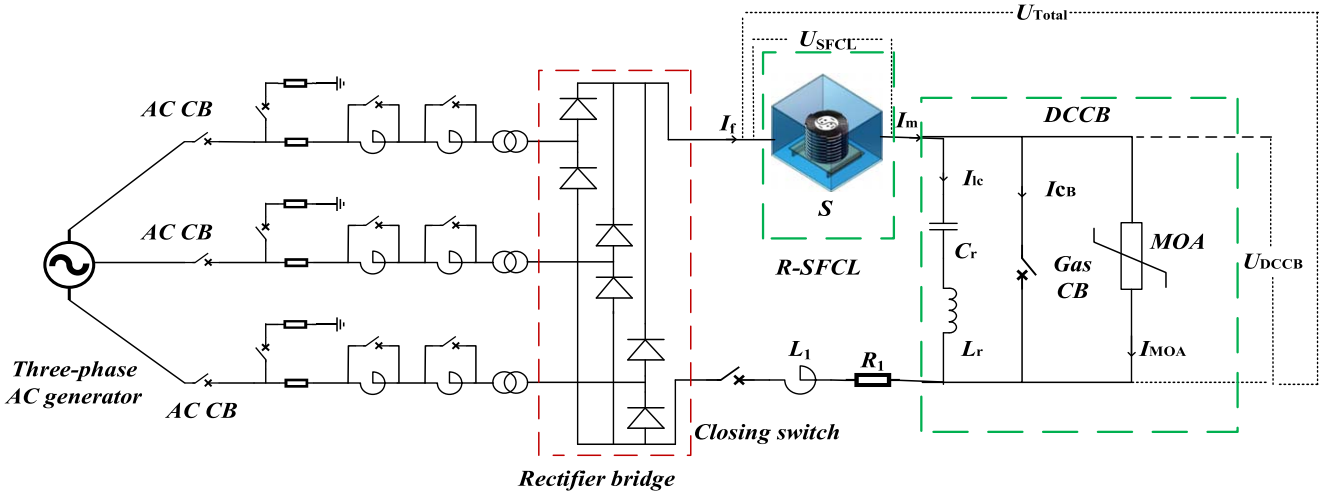

Figure 3. DC test circuit.

filled with LN_2 as shown in figure 2. The test pressure is 1 absolute atmosphere.

2.2. Design of the M-DCCB

The M-DCCB includes a nominal current branch (a SF_6 gas CB), a commutation branch (commutation capacitor C_r and commutation inductor L_r), and an energy absorption branch (metal-oxide arrester (MOA)) parallel connected as shown in figure 3. Figure 4 shows a photo of the test R-SFCL and the M-DCCB in the DC testing lab. Different from other SF_6 gas CBs, a transverse magnetic field of 200 mT is applied between the contacts of the SF_6 gas CB to increase the interruption ability of the M-DCCB [21]. The transverse magnetic field between the contacts can increase the arc voltage of the gas arc to charge C_r faster so that the arcing time of the interruption can be reduced [16]. In the normal state, the normal current transports through the nominal current branch. When a short-circuit fault occurs, the R-SFCL will respond automatically and limit the fault current. Then the M-DCCB will interrupt the limited current through the self-excited oscillation method.

The interruption principle of the M-DCCB is as follows: when a short-circuit fault occurs, a signal will trigger the moving contacts of the gas CB. Then the contacts open and an arc appears. The arc voltage increases with the increase of the gap distance between two contacts and will charge C_r. Due to the negative resistivity and instable characteristics of the gas arc, there will be an oscillating current I_{lc} as shown in figure 3 which flows through the commutation branch and the nominal current branch. The amplitude of I_{lc} increases gradually with time due to the charging of the arc voltage. Thus, the current transports in the gas CB will be the limited current I_m superimposed on the oscillating current I_{lc}. The current transports through the gas CB will have an escalating oscillation when the amplitude of I_{lc} increases during interruption. A current zero point appears when the amplitude of I_{lc} is the same or higher than the amplitude of I_m. The gas CB will interrupt the current at the current zero point. After

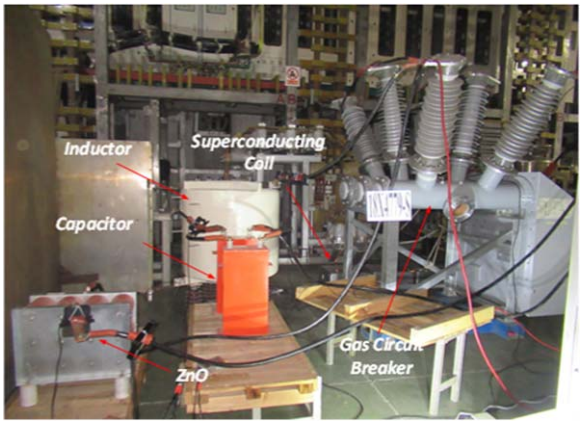

Figure 4. Photo of the R-SFCL and the M-DCCB in the testing lab.

interruption, the recovery voltage will charge C_r until the voltage of the gas CB reaches the residual voltage of the MOA. The MOA will become conductive to limit the recovery voltage and absorb the residual energy until the current in the system reduces to nearly zero. For a gas interruption, the oscillation frequency of the current usuallranges from 500 Hz to several kilohertz. When C_r changes from 10–200 μF, the arcing time is lowest when C_r is 200 μF. Thus, the value of C_r is chosen as 200 μF. The frequency of the oscillation current is approximately 1000 Hz, and the gas CB has the ability of interrupting several kiloamperes. So L_r is chosen to be 100 μH. The residual voltage of MOA is usually 1.3–1.7 times of the rated voltage in the DC system. Thus, the residual voltage of the MOA is chosen to be 15 kV, 1.5 times the testing system voltage.

2.3. Test DC circuit

Figure 3 shows the test circuit including the R-SFCL and the M-DCCB. A three-phase AC generator supplies current and voltage. A 12-pulse rectification method is used to rectify the AC to DC. The line resistor R_1 and the line inductor L_1 are used to change the amplitude and the rate of the rise of the test

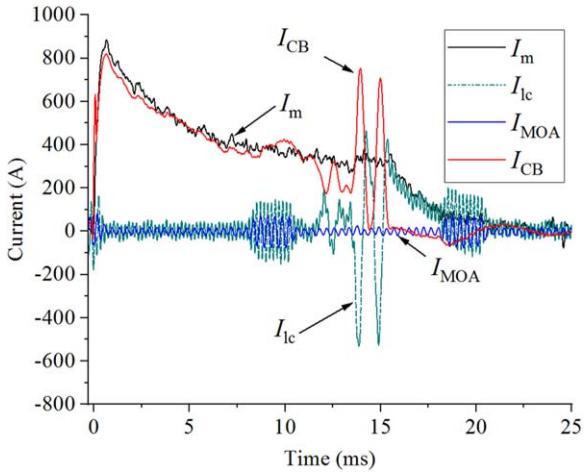

Figure 5. Current waveforms of the 3 kA/3 kV test.

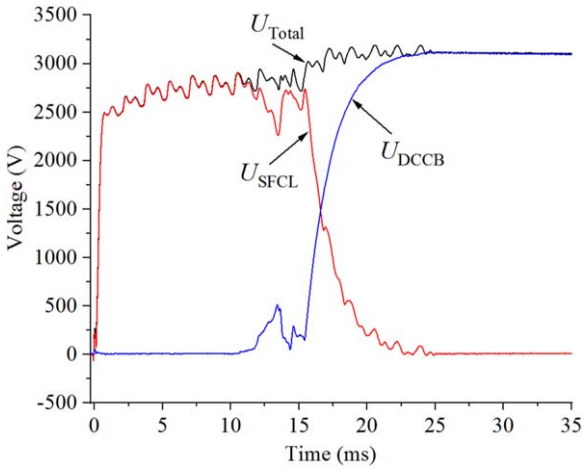

Figure 6. Voltage waveforms of the 3 kA/3 kV test.

current. A closing switch is used to switch on the circuit. The closing switch closes at zero moment to obtain a test DC current. The CBs in the AC side will also break the current after the test M-DCCB interrupts the test current to protect the circuit in case of interruption failure. The R-SFCL and the M-DCCB are connected in series. The limited current I_m, the current transports in the gas CB I_{CB}, the current transports in the commutation branch I_{lc}, and the current transports in the MOA I_{MOA} are tested by Hall sensors. The voltage of the R-SFCL U_{SFCL}, the voltage of the M-DCCB U_{DCCB}, the voltage of the R-SFCL, and the M-DCCB together U_{Total} are tested by voltage dividers. The test DC voltages are 1.3, 3, and 10 kV. The test DC current ranges from 1–10 kA which is 4.4–44 times the critical current of the test YBCO tape. The test current has a high rate of rise and a high amplitude. For example, for the 10 kV and 10 kA tests, the test current increases to 7.1 kA at 1 ms and to 9.1 kA at 2 ms. The test current flow time ranges from 30–70 ms.

3. Experimental results

3.1. DC limiting and interruption test of 3 kV/3 kA

Experiments are used to obtain the quenched resistance, the current-limiting, and interrupting characteristics of the R-SFCL and the M-DCCB. Figure 5 shows one example of the current waveforms in the 3 kV/3 kA tests. Test voltage is 3.1 kV and the test current is 3 kA, which is 13.3 times the critical current of the YBCO tape. When the test current transports through the R-SFCL, the R-SFCL will respond automatically before the fault current reaches its peak value. The fault current surpassed the critical current of the YBCO tape at approximately 0.1 ms, and the R-SFCL responded quickly and became a time-varying resistor to limit the fault current. When a fault occurred, a signal triggered the gas CB to open its moving contacts and interrupt the limited current. The R-SFCL limited the fault current of 3 kA to lower than 886 A, so the M-DCCB only needed to interrupt I_m of several hundred amperes. The current-limiting ratio (peak value of I_m divided by the fault current) reached 70.5%. I_m decreased gradually with time because the quenched resistance of the R-SFCL increased with the current flow time. At 10.5 ms, the contacts of the gas CB opened and the arc voltage started to charge C_r. Thus, I_{lc} started to increase and oscillate. When the amplitude of I_{lc} was equal to the amplitude of I_m, I_{CB} reduced to zero and the gas CB interrupted I_{CB} at the current zero point was approximately 16.4 ms. The arcing time was the time duration from the contacts opened to the arc distinguished, which was 5.9 ms in this test. The residual current reduced to zero at 21.3 ms. I_{MOA} was zero all the time because the residual voltage of the MOA was 15 kV so that the MOA could not become conductive. Interferences in I_{MOA} and I_{lc} occurred every 10 ms probably because the magnetic fields in the testing lab interfered with the Hall sensors which were used to test the current.

Figure 6 shows the voltage waveforms of the same 3 kA/3 kV test. U_{SFCL} started to increase at 0.1 ms due to the quick response of the superconducting coils. The impedance of the superconducting coils increased quickly from 0–0.7 ms. At 0.7 ms, U_{SFCL} was 2484 V. From 0–10.5 ms, U_{DCCB} was zero because the resistance of the contacts compared with the quenched resistance of the R-SFCL were very small. U_{DCCB} started to increase after the contacts opened because of the arc voltage. The R-SFCL, the M-DCCB, and the line impedance shared the system voltage from 10.5–15.4 ms. After the gas CB interrupted I_{CB}, U_{SFCL} decreased to zero and U_{DCCB} increased to the system voltage gradually. At 24.6 ms, U_{DCCB} was equal to U_{Total}. Ripples appeared on the voltage waveforms because the 12-pulse rectification method was used to rectify AC to DC.

3.2. DC limiting and interruption test of 10 kV/10 kA

Figures 7 and 8 show the current and voltage waveforms for the 10 kV/10 kA test, respectively. The test current is 10 kA. The tendency of current and voltage waveforms is same as in the 3 kV/3 kA test. The experimental results show that the R-SFCL limited the test current of 10 kA to 1416 A at 0.2 ms. The fault current-limiting ratio was 85.8%. The rate of the rise

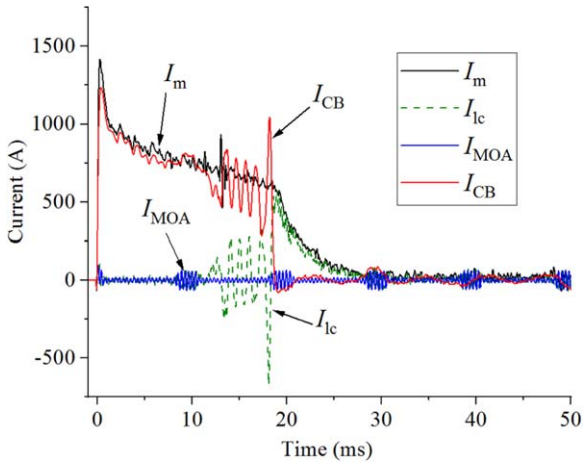

Figure 7. Current waveforms of the 10 kA/10 kV test.

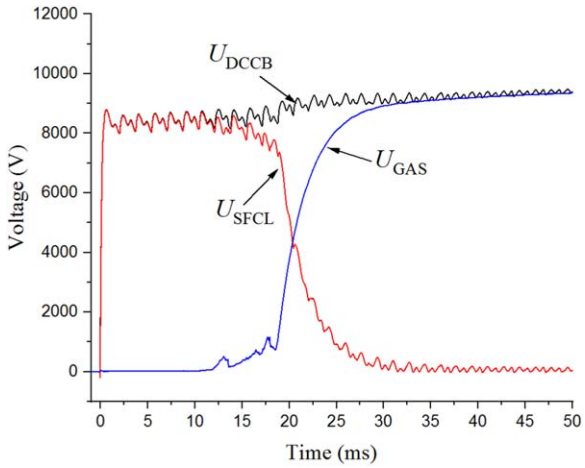

Figure 8. Voltage waveforms of the 10 kA/10 kV test.

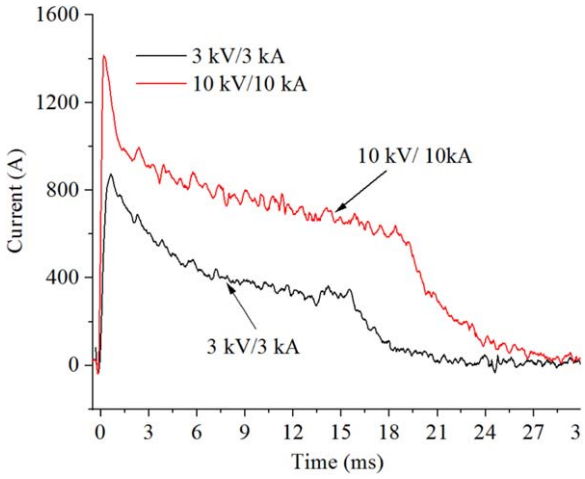

Figure 9. Effect of fault currents and system voltages on I_m.

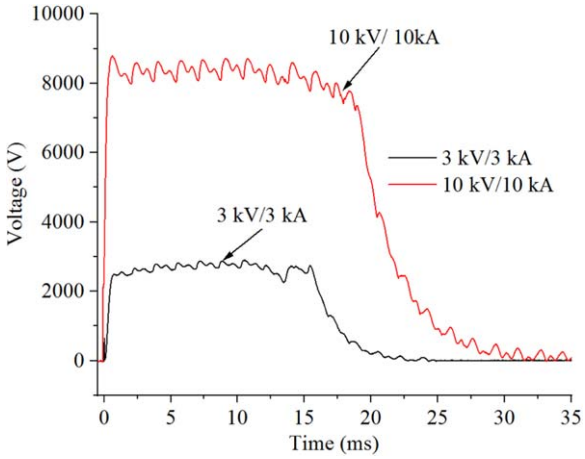

Figure 10. Effect of fault currents and system voltages on U_{SFCL}.

of the fault current was limited from 7.1–1.4 kA ms^{-1}. At 11 ms, the contacts of the gas CB opened. I_m was limited to 714 A at 11 ms, thus the gas CB only needed to interrupt a much lower current. The gas CB interrupted I_{CB} at 18.7 ms and the arcing time was 7.7 ms. Because the current needed to be interrupted the gas CB was 343 A higher than the interruption current in the 3 kV/3 kA test as shown in figure 5, and the oscillation current I_{lc} needed more time to reach the amplitude of I_m. The gap distance between the contacts will also need to be longer to obtain a higher arc voltage and thus a higher oscillation current. The peak value of I_{CB} was 1044 A which was also 291 A higher than in the 3 kV test. The MOA did not become conductive after the gas CB interrupted I_{CB}, so the residual current transported through the R-SFCL and the commutation branch.

During the interruption process, the R-SFCL and the line impedance withstood the system voltage before 11 ms. After the gas CB opened its contacts at 11 ms, the R-SFCL and the M-DCCB mainly withstood the system voltage together. The peak value of the arc voltage was 1161 V. The arc voltage increased with the increase of the gap distance. Thus for a longer arcing time, the arc voltage was also higher. After the gas CB interrupted I_{CB} at 18.7 ms, U_{SFCL} reduced to zero and U_{DCCB} increased to the system voltage gradually.

Usually there will be a high overvoltage after the gas CB interrupts the fault current. However, there was no overvoltage after the gas CB interrupted the current probably because the R-SFCL absorbed a lot of energy during the interruption and limited the fault current to a much lower value. There is no overvoltage in the interruption process in all the 10 kV/10 kA tests, thus the MOA does not operate during interruption. The residual current is transported through the R-SFCL and the commutation branch. This means that there is no need to apply the MOA in the M-DCCB when the M-DCCB is combined with an R-SFCL.

3.3. Effect of fault currents and system voltages on current-limiting

The rate of the rise and the amplitude of the fault current and the current transporting duration will influence the quenched resistance of the superconducting coils and then influence the current-limiting capacity of the R-SFCL [22]. Figures 9 and 10 show the effect of fault currents and system voltages on I_m, which is the current transports through the R-SFCL, and

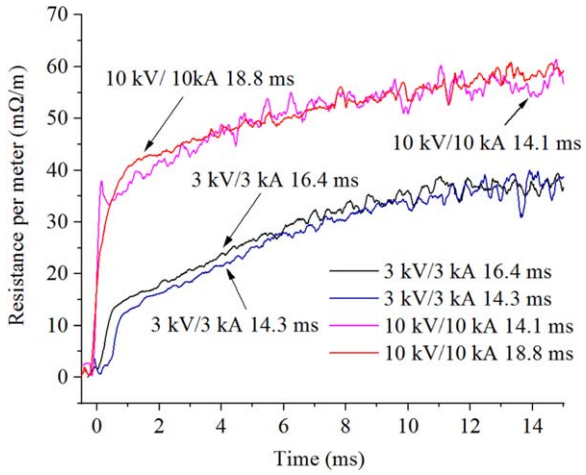

Figure 11. Effect of fault currents and system voltages on quenched resistance.

U_{SFCL} when the fault currents are 3 and 10 kA and the current transporting duration ranges from 23–30 ms. A short-circuit fault occurs at 0 ms. For the 3 kA/3 kV test, figure 9 shows that, the R-SFCL is limited I_m from 3 kA to 886 A at 0.7 ms. The gas CB interrupted I_{CB} at 16.4 ms and the current duration time was approximately 23 ms. Figure 10 shows that the peak value of U_{SFCL} was about 2849 V. For the 10 kV/10 kA interruption test, the gas CB interrupted I_{CB} at 18.8 ms and the current duration time was approximately 30 ms. The peak value of I_m was 1416 A, which was only 14.2% of the fault current. The peak value of U_{SFCL} was 8791 V. U_{SFCL} increased to 4549 V at 0.3 ms and proved the fast response of the R-SFCL. The rising rate of I_m and U_{SFCL} is higher in the 10 kV/10 kA test due to the faster rising rate of the test current in the 10 kA test. The amplitude of I_m and U_{SFCL} is also higher in the 10 kV test because the input power is larger.

For all the tests, there were no overvoltages seen after interruption probably because the R-SFCL absorbed a lot of energy. The highest voltage applied on the R-SFCL and the M-DCCB is the DC system voltage. U_{SFCL} increased with the increase of the test voltage. Thus, for a higher test voltage, the R-SFCL needs to withstand a higher voltage. Table 2 shows the value of I_m when the gas CB interrupted the current and the current-limiting ratio for the 3 and 10 kV tests. The time in the first column means the interruption time when the gas CB interrupts I_{CB}. The experimental results showed that the current needed to be interrupted by the M-DCCB increases with the fault current. For the higher fault current, the current-limiting ratio is also higher. The gas CB only needs to interrupt several hundred amperes with the help of the R-SFCL when the fault current ranges from 13.3–44 times the critical current of the YBCO tape. The difficulty of the interruption and the arcing time can be greatly reduced. The M-DCCB does not need to withstand a high overvoltage, which also make the interruption easier.

Figure 11 shows the effect of the fault currents and system voltages on the quenched resistance of the R-SFCL. The time in figure 11 also means the interruption time. The quenched resistance waveforms of the R-SFCL are calculated

Table 2. Parameters of the 3 kV and 10 kV tests.

Parameters	I_m	Current-limiting ratio
3 kV/3 kA 16.4 ms test	370 A	70.5%
3 kV/3 kA 14.3 ms test	371 A	71.3%
10 kV/10 kA 14.1 ms test	667 A	91.8%
10 kV/10 kA 18.8 ms test	714 A	85.8%

by U_{SFCL} divided by I_m. Since I_m was higher than the critical current, the quenched resistance rose rapidly to limit the fault current. In the 3 kV/3 kA 16.4 ms test, from 0–1 ms, the inductance of the superconducting coils influenced the quenched resistance waveform due to the high rising rate of the test current. After 1 ms, the waveform was mainly influenced by the quenched resistance. The quenched resistance rose sharply to 13 $m\Omega\,m^{-1}$ within 0.7 ms. After that, the rising rate of the quenched resistance slowed down and increased to 39 $m\Omega\,m^{-1}$ around 15 ms. For the 10 kV/10 kA interruption tests, the quenched resistance increased very quickly at first to 36.1 $m\Omega\,m^{-1}$ at 0.6 ms. Then the rate of the rise also reduced, and the quenched resistance increased to 59.8 $m\Omega\,m^{-1}$ at 15 ms. For the higher fault current, both the rate of the rise and the average value of the quenched resistance are higher due to the larger input energy resulting in more Joule heat to the coils. The response time was always shorter than 0.5 ms and the superconducting tapes responded faster when the fault current and the system voltage were higher.

Figure 11 shows that when the fault current and the system voltage are same, the waveforms of the quenched resistance are similar, so the quenched resistance model of the YBCO tapes in different fault conditions can be obtained. When I_m was higher than the critical current, the superconducting tapes entered a magnetic flux flow state first. During the period of 0∼1 ms, the quenched resistance was mainly determined by the YBCO layer, and the rate of rise of the quenched resistance was high. It can be obtained from the E-J characteristics of the high temperature superconductor in equation (1). E_c was 1 $\mu V\,cm^{-1}$. E was the electrical field. J was the current density. J_c was the critical current density and n was 28 for the YBCO tape. The increase of the current density caused the electric field intensity of the superconducting tapes increasing exponentially. More thermal energy was produced in the superconducting tapes due to the increase of the resistance, leading to the temperature rise. Therefore, the critical current density was reduced and the electric field intensity was further expanded to form a positive feedback. The inductance of the superconducting coils will also influence the rising rate of the fault current although the superconducting coils are in a non-inductive winding method. After 1 ms, the superconducting tapes entered the quenched state gradually and the quenched resistance depended on the resistance of the YBCO layer and the two stainless steel stabilizer layers together. As the resistance of the YBCO layer increases, the total resistance of the R-SFCL is mainly determined by the stainless steel layers because the resistance of the stainless steel layers is lower compared with that of the

Table 3. Coefficients of the fitted exponential equations.

Parameters	R_m/mΩ/m	t_1/ms	τ/ms
3 kV/3 kA 16.4 ms test	41.7	0.2	9.0
3 kV/3 kA 14.3 ms test	43.9	0.3	11.6
10 kV/10 kA 14.1 ms test	56.8	0.2	3.5
10 kV/10 kA 18.8 ms test	58.9	0.2	4.2

YBCO layer. The temperature and the current density had a smaller effect on the resistivity of the stainless steel than on the YBCO layer, so the rising rate of the quenched resistance declined over time.

$$E(J) = E_c\left(\frac{J}{J_c}\right)^n. \quad (1)$$

Exponential fitting was used to obtain the time-varying resistance waveforms of the R-SFCL. The fitted curve can be described by the exponential equation (2), where R is the resistance per meter ($m\Omega\,m^{-1}$) and t is time (ms). R_m is the maximum resistance related to the type and length of the superconducting tapes. τ is a time constant which characterizes when the resistance rises to 80% of the maximum value. t_1 is the quench-starting time determined by the flow current and the critical current of the superconducting tape.

$$R(t) = R_m[1 - e^{-\frac{t-t_1}{\tau}}]^{\frac{1}{2}}. \quad (2)$$

All the quenched resistance curves can be fitted by the exponential equation (2). Table 3 shows the equation coefficients of the fitted quenched resistance curves. A comparison of the experimental waveforms and the fitted curves are shown in figure 12. The fitted curve was different from the experimental waveforms before 1 ms because the actual curves have two distinct rising rates. After 3 ms, the exponential equation (2) can be fitted with the experimental waveforms accurately. The exponential equations of the quenched resistance can be used as the quenched resistance models of the R-SFCL in simulations because the M-DCCBs need some time, usually more than 3 ms, to react and open its contacts. Table 3 shows that R_m increased with the fault current and the system voltage. The quench-starting time t_1 is 0.2 or 0.3 ms in all the tests. The time constant τ which characterizes when the resistance rises to 80% of the maximum value decreased with the increase of the fault current.

4. Simulation of the recovery time of the R-SFCL

4.1. Numerical analysis

It is difficult to test the temperature of the superconducting coils during fast quenching and the DC interruption process, so simulation methods were used to obtain the temperature and the recovery characteristics of the R-SFCL based on the thermal conduction theory. A two-dimensional thermal conduction equation (3) is applied to calculate the temperature of the tape in the current-limiting process [13]. One dimension analyzed is the direction of the length of the tape and the other

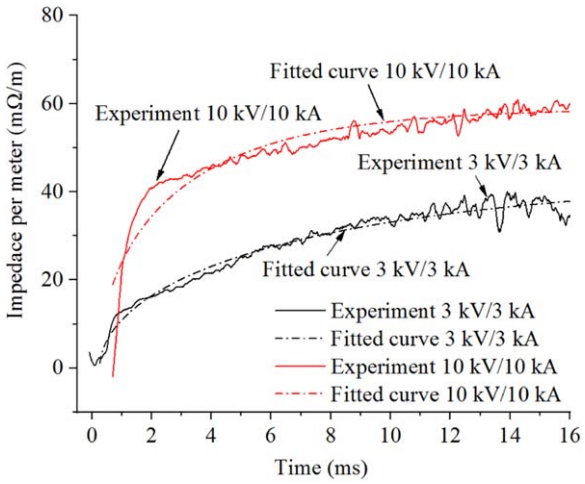

Figure 12. Comparison of the experimental and fitted waveforms.

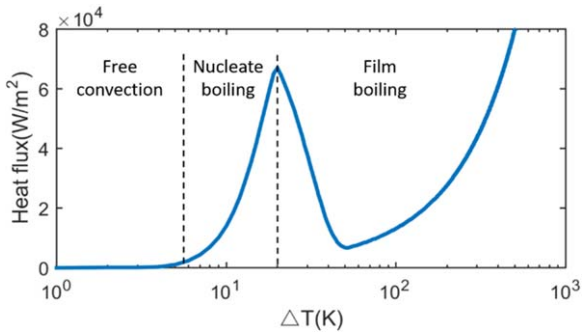

Figure 13. Pool boiling curve of the LN_2.

one is the direction of the thickness of the tape. The simulation sample is the same YBCO tape used in the experiments. The tape includes two stabilizing layers of stainless steel, a Ag layer, a YBCO layer, a buffer stack layer, and a NiW layer. The two stainless steel stabilizer layers are at the outermost layer of the tape. The thicknesses of the two stainless steel layers, the Ag layer, the YBCO layer, and the NiW layer were 75, 3, 0.8, and 75 μm, respectively. The buffer stack layer is not considered because its thickness is too small compared with other layers. Equation (4) shows the calculation method of the Joule heating g. ρ_{normal} was the average resistivity of the NiW, Ag, and the SUS layers.S_{normal} was the cross-sectional area of the NiW, Ag, and SUS layers. ρ_{SC} was the resistivity of the YBCO layer and $S_{SC}$was the cross-sectional area of the YBCO layer. The thermal conductivity κ, the volumetric heat capacity c, and the resistivity ρ of each material changed with temperature were obtained from [23–26]. The transport current through the tape was the I_m obtained from the experimental results in section 3. The background temperature was 77 K, the same as the boiling point of the LN_2 in the experiments. The cooling to the superconducting coils and the heat transfer to LN_2 calculated based on the pool boiling curve of the LN_2 are shown in figure 13. The effect of the difference in temperature ΔT between the superconducting coils and the LN_2 on the heat flux is shown in figure 13. The temperature of the superconducting tapes is mainly determined by the competition of

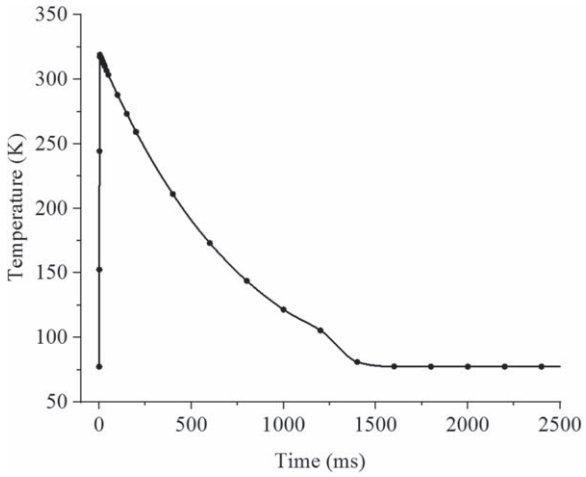

Figure 14. Temperature of the YBCO tape for the 10 kV/10 kA test.

the input Joule heat and the cooling, which is the heat transfer to LN_2.

$$c(x, y, t)\frac{\partial T}{\partial x} = \frac{\partial}{\partial x}\left[k(x, y, t)\frac{\partial T}{\partial x}\right] + \frac{\partial}{\partial y}\left[k(x, y, t)\frac{\partial T}{\partial y}\right] + W + G, \quad (3)$$

where $T(x, y, t)$ is the temperature (T), $k(x, y, t)$ is the thermal conductivity ($W/m \cdot K$), $W(x, y, t)$ is the heat transfer to liquid cooling (W/m^3), $G(x, y, t)$ is the Joule heat (W/m^3), and $c(x, y, t)$ is the volumetric heat capacity ($J/m^3 \cdot K$).

$$g = \frac{\rho_{\text{normal}} \cdot I_{\text{normal}}^2}{S_{\text{normal}}} + \frac{\rho_{sc} \cdot I_{\text{SC}}^2}{S_{\text{sc}}}. \quad (4)$$

4.2. Recovery time of the R-SFCL

Figure 14 shows the temperature of the YBCO tape when the gas CB interrupted the current at 14.1 ms in the 10 kV/10 kA test. The current transported through the YBCO tape is obtained from I_m as shown in figure 9. The current flow time of I_m is 25.6 ms. The simulation results show that the temperature of the YBCO tape increased very quickly at first from a bath temperature of 77 K to a high level when the transport current was applied. The peak value of the temperature was 319.0 K. The temperature at the outermost layers of the tape was lower than the temperature at the middle layers of the tape because the two outermost layers (stainless steel layers) contacted the LN_2 directly. The simulation results show that the difference in temperature at each layer is small because the thickness of the tape is very thin. The temperature of the superconducting coils increases very quickly during the quench. The difference in the temperature of the superconducting coils and LN_2 is large, which can be larger than 200 K when the fault current is higher than 3 kA. Thus, the boiling of the LN_2 changes from nucleate boiling to film boiling within a short time. The temperature of the YBCO tape decreased continuously when I_m reduced to zero. The temperature of the tape reduced to 105.4 K at 1.2 s, to 80.9 K at 1.4 s, and to 77 K at 1.6 s. During the recovery period, only the cooling effect determines the temperature because the transported current is stopped. The rate of the decrease of the temperature is influenced by the relationship between the heat flux and ΔT. When ΔT is approximately 45 K, there is an inflection point in the pool boiling curve of the LN_2. And there is also an inflection point of approximately 122 K as shown in figure 14 probably due to the transition of heat flux near 45 K. The temperature of the tape reduced to 80.9 K at 1.4 s, so the recovery time of the tape for the 10 kV/10 kA test was approximately 1.3 s.

Table 4. Comparison of temperature and recovery time.

Test current	Average value of I_m	Current flow time	Highest temperature	Recovery time
1 kA	364.7 A	10.1 ms	95.6 K	9.9 ms
3 kA	514.8 A	23.0 ms	295.5 K	1.1 s
10 kA	603.8 A	25.6 ms	319.0 K	1.3 s

Other tests of 1, 3, and 10 kV are also simulated by the numerical analysis using the same method. Table 4 shows the relationship between the average value of the I_m, the maximum temperature of the YBCO tape, and the recovery time of the R-SFCL. As shown in the first row in table 4, the superconducting tapes did not quench completely because the average value of the I_m was only 1.6 times the critical current. Besides, the current flow time was only 10.1 ms. Thus the highest temperature of the tape was only 95.6 K and it recovered soon after 9.9 ms. The simulation results show that when the fault current is higher than 3 kA (13.3 times the critical current), the recovery time is usually more than 1 s. The highest temperature and the recovery time increase with the increase of the fault current. If HVDC systems have an open-close-open requirement, research should be done to reduce the recovery time such as increasing the interruption ability of the DCCB, decreasing the interruption time, enhancing cooling, and increasing the heat dissipation area.

5. Simulation of the R-SFCL and the M-DCCB in the MMC-MTDC Grid

5.1. Simulation setup

The characteristics of the R-SFCL and the M-DCCB installed in MMC-based MTDC grids were simulated to study the current-limiting and interrupting effects of the R-SFCL and the M-DCCB in MMC-MTDC grids by PSCAD/EMTDC software. Figure 15 shows an MMC-MTDC grid model from the CIGRE B4-57 working group, which is used to investigate the short-circuit fault current interruption of the R-SFCL and the DCCB in a four-terminal VSC-HVDC system. The R-SFCL and the M-DCCB were combined and shown as the DC circuit breaker (blue circle) in figure 15 to save the place. A solid pole-to-pole fault, i.e. F1–F8, was simulated because it was the most severe fault in this grid. When a fault occurs at

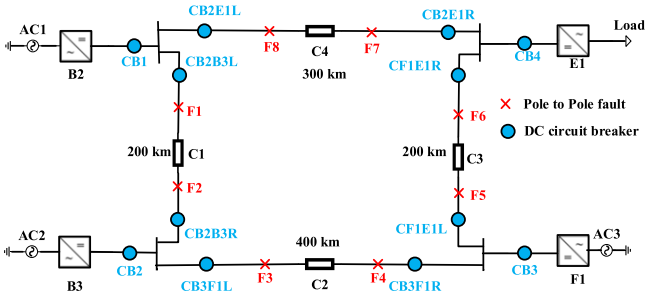

Figure 15. MMC-MTDC grid model.

Table 5. Main parameters of the MMC-MTDC grid.

Parameters	B2	B3	F1	E1
AC voltage/kV	220	220	220	220
AC frequency/Hz	50	50	50	50
DC voltage/kV	±200	±200	±200	±200
DC current/A	800	800	800	800
Control mode	PVDC/Q	PVDC/Q	P/Q	Vac/f
Number of SM	400 per phase			
Arm inductance/mH	29	20	29	116
SM capacitance/mF	10	15	10	25

the cable end, the corresponding DC circuit breaker and the converter station face the most severe scenario. Thus, all eight severe fault locations, F1–F8, were studied for DC protection. The main parameters of the grid are listed in table 5. To protect the converter stations, they are blocked when the DC current exceeds 6 kA.

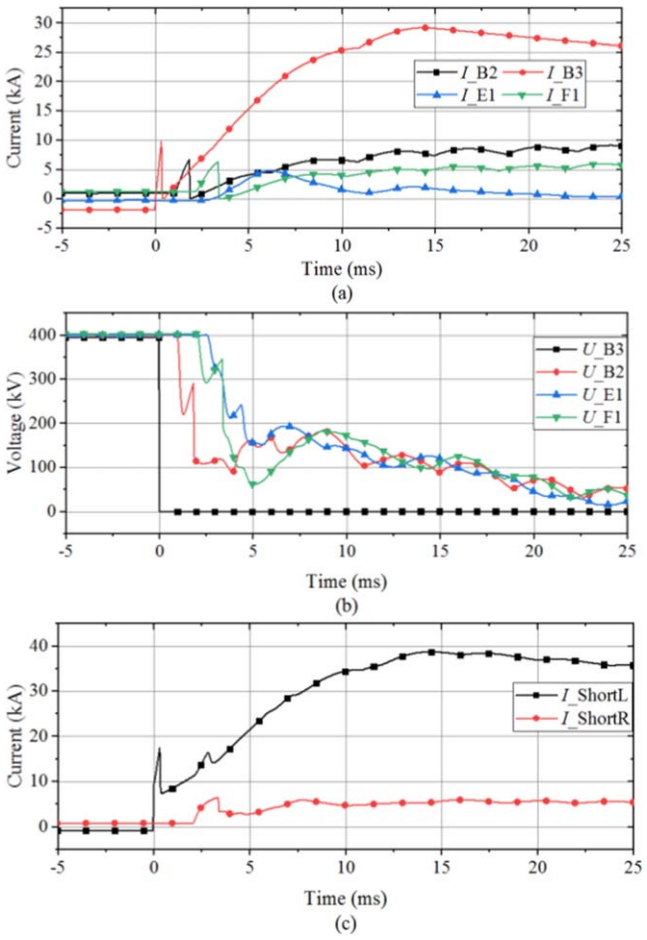

Figure 16. (a) Converter station current, (b) converter station voltage, (c) current on both sides of the fault point.

5.2. Simulation results

Figure 16 shows a bipolar DC fault when the R-SFCL and M-DCCB are not installed in the grid. The fault occurred at F3 in the grid. After the fault occurred, the converter station discharged to the fault point. The high fault current caused converters B2, B3, and F1 to be locked within 5 ms, and the system power was then interrupted. Figure 16(a) shows the current of the four converters. Figure 16(b) shows the voltage of the four converters. Figure 16(c) shows the fault current at the left named *I*_ShortL and at the right named *I*_ShortR. Figure 16(a) shows that the fault current of converter B3 increased to 29.2 kA at 14.35 ms. There was a peak value of 9.8 kA at 0.3 ms. After 0.3 ms, the current of converter B3 increased gradually to 29.2 kA and decreased slowly to 26.14 kA at 25 ms. The other converter currents were lower than 10 kA all the time. The voltage of converter B2 decreased to 221.7 kV at 1.25 ms. The voltage of B2 started to decrease at 1 ms. The voltages of F1 and E1 started to decrease at 2.0 and 2.5 ms. The decreasing rate was very high. From 5–25 ms, the voltage of the converters ranged from 400–0 kV. The peak value of the fault current on the left side of the fault point was 38.75 kA and was 6.47 kA on the right side. The fault was near converter B3, so the voltage drop was large when the short-circuit fault occurred. All the converters were blocked, and the power transmission were stopped. A substantial amount of power was lost after the short-circuit fault.

The R-SFCL and the M-DCCB (referred to as the DC circuit breaker in figure 15) were installed in the MMC-MTDC grid to interrupt the fault current. When a short-circuit fault occurred at F3, DC circuit breakers CB3F1L and CB3F1R in figure 15 isolated the fault. The quenched resistance of the superconducting coils of the R-SFCL were obtained from the 10 kV/10 kA experiment. The rated current of cable C2 was 800 A. The critical current of the superconducting tapes was 225 A, so at least four YBCO tapes should be connected in parallel to ensure that the YBCO tapes remained in a superconducting state during normal conditions. The quenched resistance is proportional to the length of the tape. In order to obtain the same quenched resistance per meter and voltage per meter as in the experiments, the length of the single tape should be multiplied by 20 (200 kV/10 kV to get same voltage per meter) then by 4 (four tapes in parallel). So the withstanding voltage per meter of the superconducting tape was the same as it was in the experiments. C_r was also set as 200 μF, and L_r was set as 100 μH, the same as in the experiments. The Mayr arc model shown in

equation (5) was used to simulate the gas arc [16].

$$\frac{dg}{dt} = \frac{g}{\theta}\left(\frac{iu}{N} - 1\right), \tag{5}$$

where N is the power loss coefficient (W), θ is the arc time constant (s), g is the arc conductance (S), i is the arc current, and u is the arc voltage.

Figure 17 shows the current and voltage waveforms when the R-SFCL combined with the M-DCCCB were applied in the grid. Figures 17(a) and (b) show the currents and voltages, respectively, of the four converters. Figures 17(c) and (d) show the current waveforms in each branch of breakers CB3F1L and CB3F1R, respectively. I_f is the fault current transport through the R-SFCL. I_{CB} is the current transports in the gas CB. I_{lc} is the current transports in the commutation branch. Figure 17(e) shows the voltage of breakers CB3F1L and CB3F1R. The currents in all the converters were lower than 4.25 kA due to the quick response and the high quenched resistance of the superconducting coils. The absolute values of all the currents were less than 2 kA after 26.6 ms. All the currents became stable after 100 ms. The system voltages of all the converters were higher than 300 kV. Thus, the R-SFCL combined with the M-DCCB effectively delayed the voltage drop. The voltage of converter B3 dropped to 325 kV at 17 ms. All the voltages were nearly stable after 50 ms.

Figures 17(c) and (d) show that the current peak value of the breaker CB3F1L was 9.5 kA. After 1 ms, the fault current I_f was less than 5.2 kA, and the M-DCCB only needed to interrupt a current of 4.3 kA. The arcing time was 8.6 ms. The fault current of breaker CB3F1R increased to 3.8 kA at 3.4 ms. Breaker CB3F1R needed to interrupt a current of 3.8 kA. The current was interrupted when the commutation current reached the amplitude of the fault current. The arcing time was approximately 4 ms. The arcing time and the difficulty of the interruption decreased substantially because the R-SFCL limited the fault current to a very low level. There was no overvoltage after the interruption in the simulations, which agreed with the experimental results, probably because the R-SFCL limited the fault current to a much lower value and absorbed a substantial amount of energy during interruption. After the gas CB interrupted the fault current, the voltage of CB3F1L and CB3F1L increased quickly, and then remained stable at system voltage. With the help of the R-SFCL and the M-DCCB installed in the MMC-MTDC grid, all the converters were blocked during the short-circuit faults. Thus, the power in the healthy cable can be continuously transmitted.

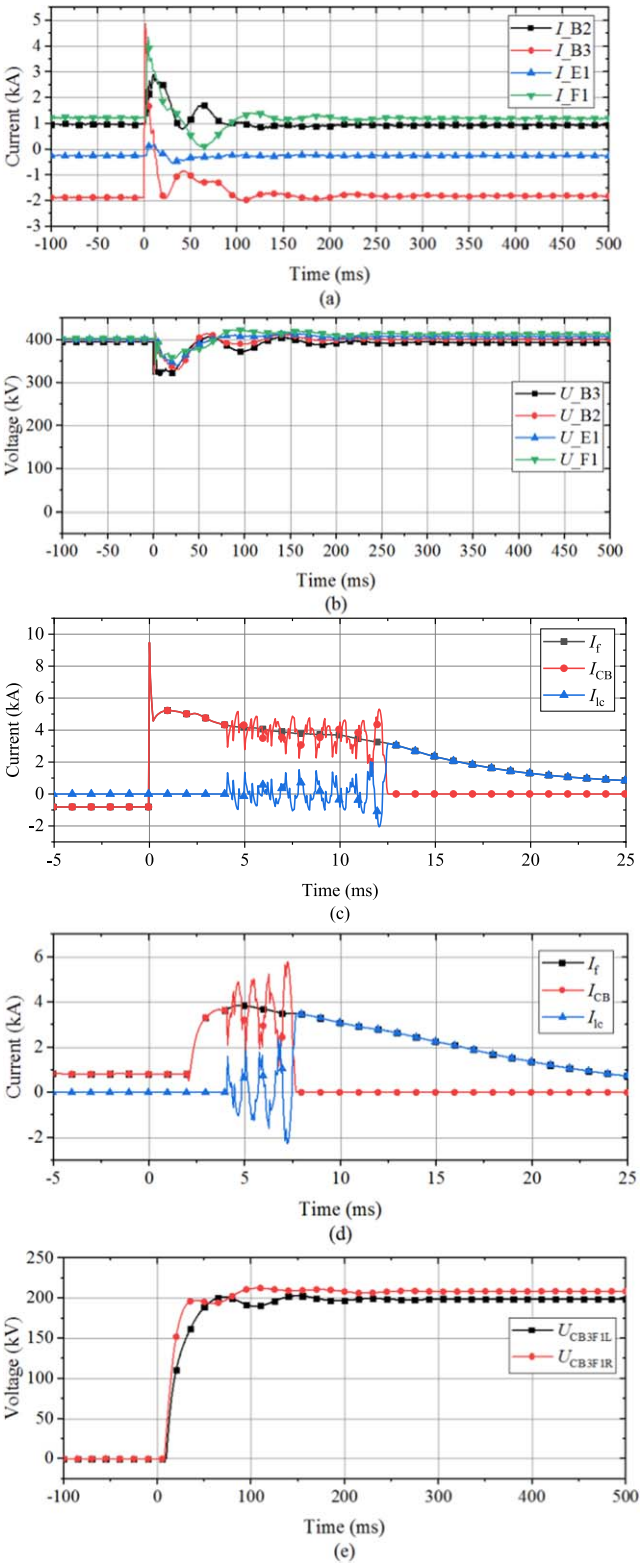

Figure 17. (a) Converter station current, (b) converter station voltage, (c)current in each branch of the breaker CB3F1L, (d) current in each branch of the breaker CB3F1R, (e) voltages of the breakers CB3F1L and CB3F1R.

6. Conclusion

In this paper, the short-circuit fault current-limiting characteristics of a designed R-SFCL combined with a mechanical-type DCCB (M-DCCB) in DC grids are obtained.

(1) The designed R-SFCL combined with the M-DCCB based on the self-excited oscillation interruption principle limited a 10 kA DC to the peak value of 1416 A and then interrupted the limited current in a 10 kV DC circuit successfully.

(2) The R-SFCL has a quick response. The response time of the R-SFCL is less than 0.3 ms when the fault current is higher than 3 kA which is 13.3 times the critical current of the YBCO tape.
(3) The R-SFCL can limit the fault DC to a low level. The current-limiting ratios are always higher than 70% when the fault current is higher than 13.3 times the critical current of the YBCO tape. Thus, the difficulty of the interruption and the arcing time of the M-DCCB are greatly reduced.
(4) The numerical analysis results show that when the fault current is higher than 3 kA, the recovery time of the R-SFCL is more than 1 s. Thus, some solutions should be investigated to reduce the recovery time.
(5) The R-SFCL can effectively delay the voltage drop in MMC-MTDC grids, and provide enough time for the M-DCCB to interrupt lower limited current. With the help of the R-SFCL, other power equipment does not need to withstand high short-circuit fault currents in DC systems. Besides, there is no overvoltage after interruption. The R-SFCL only needs to withstand the DC system voltage during interruption and the M-DCCB also does not need to withstand high overvoltage.

The successful interruption of the 10 kA fault current in the 10 kV DC circuit shows that the combination of R-SFCLs and M-DCCBs might be an effective method to interrupt short-circuit fault currents in medium voltage and HVDC grids.

Acknowledgments

This work was supported by the National Natural Science Foundation of China (Nos. 51907153, 51877166, 51911530195) and the China Postdoctoral Science Foundation (No. 2019M653632).

ORCID iDs

Bin Xiang https://orcid.org/0000-0002-9720-395X

References

[1] Chang B *et al* 2015 Multi-terminal VSC-HVDC pole-to-pole fault analysis and fault recovery study *Proc. 11th IET Int. Conf. AC DC Power Transm. (ACDC) (Birmingham)* pp 1–8
[2] Chen L *et al* 2015 Comparative study of inductive and resistive SFCL to minigate the DC fault current in a VSC-HVDC system integrated with wind power farms *Proc. of 2015 IEEE Int. Conf. on Applied Superconductivity and Electromagnetic Devices (Shanghai, China)*
[3] Chen L *et al* 2016 Comparison of inductive and resistive SFCL to robustness improvement of a VSC-HVDC system with wind plants against DC fault *IEEE Trans. Appl. Supercond.* **26** 5603508
[4] Lee H Y *et al* 2019 Appropriate protection scheme for DC grid based on the half bridge modular multilevel converter system *Energies* **12** 1837
[5] Liang S Y *et al* 2018 Tests and analysis of a small-scale hybrid-type DC SFCL prototype *IEEE Trans. Appl. Supercond.* **28** 5602106
[6] Liang S Y *et al* 2017 Study on the current limiting performance of a novel SFCL in DC systems *IEEE Trans. Appl. Supercond.* **27** 5601106
[7] Li B *et al* 2016 Studies on the application of R-SFCL in the VSC-based DC distribution system *IEEE Trans. Appl. Supercond.* **26** 5601005
[8] Yang Q Q *et al* 2017 Design and application of superconducting fault current limiter in a multiterminal HVDC system *IEEE Trans. Appl. Supercond.* **27** 3800805
[9] Larruskain D M *et al* 2012 Fault current limiters for VSC-HVDC systems *Proc. 10th IET Int. Conf. AC DC Power Transm. (ACDC)* pp 1–6
[10] Chen L *et al* 2019 Application and design of a resistive-type superconducting fault current limiter for efficient protection of a DC microgrid *IEEE Trans. Appl. Supercond.* **29** 5600607
[11] Xiao L S *et al* 2018 Research on application and configuration of SFCL in VSC-HVDC of CSG *2nd IEEE Conf. on Energy Internet and Energy System Integration (EI2)* (https://doi.org/10.1109/EI2.2018.8582312)
[12] Saldana G *et al* 2018 Impact of a resistive superconductive fault current limiter in a multi-terminal HVDC Grid *2018 19th IEEE Mediterranean Electrotechnical Conf. (MELECON)* (https://doi.org/10.1109/MELCON.2018.8379062)
[13] Xiang B *et al* 2019 Influencing factors on quench and recovery of YBCO tapes for DC superconducting fault current limiter *IEEE Trans. Appl. Supercond.* **29** 5600806
[14] Xia D *et al* 2018 Magnetic field and characteristic analysis of the superconducting fault current limiter for DC applications *IEEE Trans. Appl. Supercond.* **28** 5601405
[15] Zha W *et al* 2020 Quench and recovery characteristics of solenoid and pancake SFCLs under DC impact current *IEEE Trans. Appl. Supercond.* **30** 5600106
[16] Xiang B *et al* 2019 Effects of short circuit currents on quench and recovery properties of YBCO tapes for DC SFCL *IEEE Trans. Appl. Supercond.* **29** 5600706
[17] Yang K *et al* 2018 Direct-current vacuum circuit breaker with superconducting fault-current limiter *IEEE Trans. Appl. Supercond.* **28** 5600108
[18] Yang K *et al* 2019 A self-charging artificial current zero DC circuit breaker based on superconducting fault current limiter *IEEE Trans. Appl. Supercond.* **29** 5600505
[19] Junaid M, Xiang B *et al* 2019 Experimental test of superconductor fault-current switchgear using liquid nitrogen as the insulation and arc-quenching medium *IEEE Trans. Appl. Supercond.* **29** 5000804
[20] Xiang B *et al* 2015 DC circuit breaker using superconductor for current limiting *IEEE Trans. Appl. Supercond.* **25** 5600207
[21] Xiang B *et al* 2018 DC interrupting with self-excited oscillation based on superconducting current-limiting technology *IEEE Trans. Power Delivery* **33** 529–36
[22] Xiang B *et al* 2017 DC-current-limiting characteristics of YBCO tapes for DC currents of 50 A to 10 kA *IEEE Trans. Appl. Supercond.* **27** 5600605
[23] Smith D R *et al* 1995 Low-temperature properties of silver *J. Res. Natl. Inst. Stand. Technol* **100** 119
[24] Manfreda G 2011 Review of ROXIE's material properties database for quench simulation *Technology Department Magnets, Superconductors and Cryostats, EDMS Nr* 1178007
[25] Zhang Y F *et al* 2014 Progress in production and performance of second generation (2G) HTS wire for practical applications *IEEE Trans. Appl. Supercond.* **24** 7500405
[26] Naito T *et al* 2010 Thermal conductivity of YBCO coated conductors fabricated by IBAD-PLD method *Supercond. Sci. Technol.* **23** 105013 (4pp)